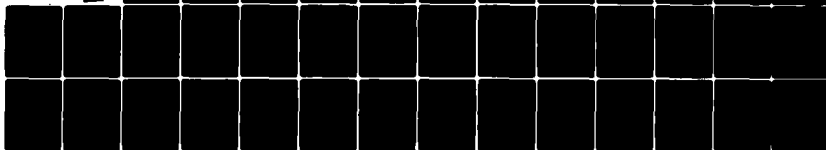AD-A095 047   CASE WESTERN RESERVE UNIV CLEVELAND OH CASE LABS FOR--ETC F/G 7/4
                DEPOLARIZED RAYLEIGH LIGHT SCATTERING STUDIES OF CONCENTRATED A--ETC(U)
                DEC 80 R A CARPIO, M MEHICIC, E YEAGER   N00014-75-C-0557
UNCLASSIFIED   TR-47   NL

1 OF 1
AD
A0 95047

END
DATE
FILMED
3-81
DTIC

OFFICE OF NAVAL RESEARCH

Contract N00014-75-C-0557
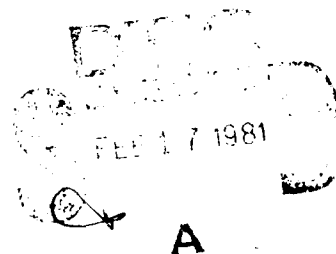
Project NR 384-305

TECHNICAL REPORT NO. 47

DEPOLARIZED RAYLEIGH LIGHT SCATTERING STUDIES OF
CONCENTRATED AQUEOUS NITRATE SOLUTIONS

by

Ronald A. Carpio, Mehmed Mehicic and Ernest/Yeager

Ultrasonic Research Laboratory
and
Case Laboratories for Electrochemical Studies
Case Institute of Technology
Case Western Reserve University
Cleveland, Ohio 44106

/   15 December 1980

A

81 2   17 008

REPORT DOCUMENTATION PAGE		READ INSTRUCTIONS BEFORE COMPLETING FORM
1. REPORT NUMBER 47	2. GOVT ACCESSION NO. AD-A095047	3. RECIPIENT'S CATALOG NUMBER
4. TITLE (and Subtitle) DEPOLARIZED RAYLEIGH LIGHT SCATTERING STUDIES OF CONCENTRATED AQUEOUS NITRATE SOLUTIONS		5. TYPE OF REPORT & PERIOD COVERED Technical Report
		6. PERFORMING ORG. REPORT NUMBER
7. AUTHOR(s) Ronald A. Carpio, Mehmed Mehicic and Ernest Yeager		8. CONTRACT OR GRANT NUMBER(s) N00014-75-C-0557
9. PERFORMING ORGANIZATION NAME AND ADDRESS Ultrasonic Research Laboratory Case Western Reserve University Cleveland, Ohio 44106		10. PROGRAM ELEMENT, PROJECT, TASK AREA & WORK UNIT NUMBERS NR384-305
11. CONTROLLING OFFICE NAME AND ADDRESS Office of Naval Research Physics Section -Code 421 Arlington, Virginia 22217		12. REPORT DATE 15 December 1980
		13. NUMBER OF PAGES
14. MONITORING AGENCY NAME & ADDRESS(If different from Controlling Office)		15. SECURITY CLASS. (of this report) Unclassified
		15a. DECLASSIFICATION/DOWNGRADING SCHEDULE

16. DISTRIBUTION STATEMENT (of this Report)

Approved for public release; distribution unlimited

17. DISTRIBUTION STATEMENT (of the abstract entered in Block 20, if different from Report)

18. SUPPLEMENTARY NOTES

19. KEY WORDS (Continue on reverse side if necessary and identify by block number)

Viscoelastic systems, Rayleigh light scattering, nitrate solutions, concentrated electrolytes, reorientational relaxation

20. ABSTRACT (Continue on reverse side if necessary and identify by block number)

Interferometric measurements of the reorientational relaxation time τ of the nitrate anion in concentrated aqueous calcium nitrate and zinc nitrate solutions have been made as a function of temperature and composition. Arrhenius plots of τ for $Ca(NO_3)_2 \cdot X\ H_2O$, where X = 4, 5, and 5.6 and $Zn(NO_3)_2 \cdot 5\ H_2O$ are linear and yield activation energies in the range of 5.6 to 8.3 Kcal/mole. The data for $Ca(NO_3)_2 \cdot 3.91\ H_2O$, which cover the most extensive range of viscosity and temperature, were non-Arrhenius and were best fitted by the

DD $_{1\ JAN\ 73}^{FORM}$ 1473 EDITION OF 1 NOV 65 IS OBSOLETE

S/N 0102-LF-014-6601

Unclassified

Continuation (Block #20)

Vogel-Tamman-Fulcher equation from which an ideal glass transition temperature was derived. The viscosity dependence of τ for both the $Ca(NO_3)_2$ and $Zn(NO_3)_2$ solutions was found to be between that predicted by the classical Stokes-Einstein equation and that predicted using slip hydrodynamic boundary conditions. Nitrate rotation was found to be slower in $Ca(NO_3)_2$ solutions than in the corresponding $Zn(NO_3)_2$ solutions.

TABLE OF CONTENTS

Page

-iv-

LIST OF FIGURES

LIST OF TABLES

DEPOLARIZED RAYLEIGH LIGHT SCATTERING
STUDIES OF CONCENTRATED AQUEOUS NITRATE SOLUTIONS

Ronald A. Carpio[a], Mehmed Mehicic[b], and Ernest Yeager
Department of Chemistry, Case Western Reserve University, Cleveland, Ohio

ABSTRACT

Interferometric measurements of the reorientational relaxation time τ of the nitrate anion in concentrated aqueous calcium nitrate and zinc nitrate solutions have been made as a function of temperature and composition. Arrhenius plots of τ for $Ca(NO_3)_2 \cdot X\ H_2O$, where $X = 4$, 5, and 5.6 and $Zn(NO_3)_2 \cdot 5\ H_2O$ are linear and yield activation energies in the range of 5.6 to 8.3 Kcal/mole. The data for $Ca(NO_3)_2 \cdot 3.91\ H_2O$, which cover the most extensive range of viscosity and temperature, were non-Arrhenius and were best fitted by the Vogel-Tamman-Fulcher equation from which an ideal glass transition temperature was derived. The viscosity dependence of τ for both the $Ca(NO_3)_2$ and $Zn(NO_3)_2$ solutions was found to be between that predicted by the classical Stokes-Einstein equation and that predicted using slip hydrodynamic boundary conditions. Nitrate rotation was found to be slower in $Ca(NO_3)_2$ solutions than in the corresponding $Zn(NO_3)_2$ solutions.

[a] To whom requests for reprints should be sent

Present address: Frank J. Seiler Research Laboratory
(Air Force Systems Command)
United States Air Force Academy, CO 80840

[b] Present address: Standard Oil Company Research Laboratory
Cleveland, Ohio 44128

I. INTRODUCTION

In this paper we report on deploarized Rayleigh light scattering studies of concentrated $Ca(NO_3)_2$ and $Zn(NO_3)_2$ solutions. These studies were undertaken in order to gain further insight into the structure and dynamics of these liquids. In an earlier paper, dealing with these same liquids as well as concentrated aqueous $ZnCl_2$ solutions, we outlined the information which could be derived from ultrasonic and hypersonic absorption coefficient measurements - the latter being derived from the polarized light scattering spectrum (1).

We are placing emphasis upon this class of liquids because they afford a bridge between dilute aqueous solutions on one end of the scale and molten salts on the other end. In fact, there is some question as to whether unique stoichiometries such as $Ca(NO_3)_2 \cdot 4\ H_2O$, $Mg(NO_3)_2 \cdot 6\ H_2O$, etc. can be considered as fused salt analogs (2). A number of these liquids can be rather easily supercooled, and thus they are convenient media for studying the metastable region of the liquid state. A favorite among investigators has been $Ca(NO_3)_2 \cdot 4\ H_2O$, which has a melting point of 42.7°C and can be readily supercooled. In fact, $Ca(NO_3)_2 \cdot 4\ H_2O$ has now been explored by the majority of available physico-chemical techniques. Reviews of work in this area can be found elsewhere (3,4). In addition, it now appears that $Ca(NO_3)_2$ solutions will become important solvents for electrochemical studies (5-7).

In this study in which Fabry-Perot interferometry is employed, we are limiting our attention to the sharp central depolarized Rayleigh component which is centered at the laser frequency and which is attributable to molecular reorientation of permanently anisotropic species (8). The much broader and less understood Rayleigh wings, due to light scattering from induced

anisotropy, appear in our spectral recordings only as a flat background upon which the central component is superimposed. From the wo : of Prorvin (9), conducted with rather low-resolution instrumentation, it was shown that the central depolarized Rayleight component of aqueous nitrate solutions arises largely from rotational motion of highly anisotropic NO_3^- anions.

Currently there is a great deal of interest being focused on the dependence of the rotational reorientation time upon shear viscosity (10). In the majority of depolarized light scattering studies which were conducted on pure, molecular organic liquids and liquid mixtures, it has been found that for constant temperature experiments the rotational reorientation times could be fit to the following equation

$$\tau = C\eta_s + \tau_0 \tag{1}$$

where η_s is the shear viscosity, C is a parameter (i.e., the degree of trans-lation - rotation coupling) and τ_0 is the zero viscosity intercept; whereas, for temperature dependence studies, the following equation was applicable (8)

$$\tau = C' \frac{\eta_s}{T} + \tau_0' \tag{2}$$

The experimental values of C or C' have been compared with the values arrived at using the hydrodynamic model with both "stick" and "slip" boundary conditions. Stick boundary conditions were those utilized in deriving the familiar Stokes-Einstein equation

$$\tau = \frac{V\eta_s}{kT} \tag{3}$$

where V is the effective molecular volume of the rotating molecule which is assumed to be spherical and k is the Boltzman constant (11). The solvent molecules are assumed to "stick to" and rotate with the solute molecules. Perrin derived equations using stick boundary conditions which apply to

2

either prolate or oblate ellipsoids (12). These equations predict that the friction coefficients, f, for an ellipsoid will be greater than the friction coefficients of a sphere of equal volume, f_0; the difference will depend upon the ratio of the major axis, a, to the minor axis, b, of the ellipsoid. With these modifications Equation (3) becomes

$$\tau = \frac{V\eta_s}{kT} \left(\frac{f}{f_0}\right) \tag{4}$$

the ratio $\left(\frac{f}{f_0}\right)$ is given graphically as a function of $\left(\frac{a}{b}\right)$ in an article by Edward (13). In general, the stick boundary conditions predict too high a value of C or C'; i.e., they predict too much friction. It should also be noted that the hydrodynamic approximation is only strictly applicable to large particles in a medium composed of small molecules. Furthermore, neither Equations (3) or (4) allow for a non-zero intercept which has been found experimentally in many cases (14-17). This non-zero intercept is not clearly understood at present, but it is thought to be associated with inertial effects. In certain cases τ_0 has been found to be similar but generally slower than the classical free rotator correlation time given by Bartoli and Litovitz (18),

$$\tau_{FR} = \left(\frac{41}{360}\right) 2\pi \left(\frac{I}{kT}\right)^{\frac{1}{2}} \tag{5}$$

where I is the moment of inertia.

When the hydrodynamic approximation is used with "slip" boundary conditions, it is assumed that the resistance arises entirely from the fact that the non-spherical object sweeps out a volume as it rotates or translates, thereby displacing a certain amount of fluid. Calculations using the slip model of rotational diffusion for prolate and oblate ellipsoids have been reported by Hu and Zwanzig (19) and for generalized ellipsoids by Youngren and Acrivos (20).

The stick boundary conditions appear to hold for large solute molecules. However, as the size of the solute molecules approach that of the solvent, the slip conditions become more applicable. In the absence of strong solvent-solute interactions, the slip conditions also give better agreement with experimental results (21). No comparisons have been reported for aqueous solutions.

II. EXPERIMENTAL

Details of the light scattering spectrometer are given elsewhere (1). Measurements of the depolarized Rayleigh spectrum were made at a scattering angle of 90°. In order to obtain the depolarized spectrum, the electric vector of the single longitudinal mode argon ion laser beam, oriented in the vertical direction, was rotated 90° with a half-wave plate, preceding the sample and fabricated for 5145 $\overset{o}{A}$ radiation. A polarizing filter (Polaroid) with the extinction ratio of 10^{-4}, located in the path of the scattered light before the Fabry-Perot interferometer, was oriented to pass only the vertically polarized component. As pointed out by Rank et al. (22), this arrangement eliminates problems with polarization dependent optics. The setting of the half-wave plate was established with the aid of a Glan-Thompson polarizer (extinction ratio 10^{-3}). The alignment of the Polaroid sheet was made by setting the incident beam for horizontal polarization with the half-wave plate and then by rotating the Polaroid until the intensity of the Rayleigh component arising from the light elastically scattered by an aqueous suspension of polystyrene spheres was minimized.

Details of the sample preparation and analysis have been given in an earlier publication (1). Bubbles were especially troublesome in these viscous solutions (23), and difficult to eliminate. Bubbles and dust were eliminated

4

by filtration through 0.1 μ Nucleopore filters held in a Teflon holder. Pressure to the filtrant was exerted by a piston filtration unit (Creative Scientific Equipment Corporation of Long Beach, California). Only those samples which appeared free of Tyndall scattering to the eye in the high intensity argon ion laser beam were employed in these studies. If the filtered solutions were allowed to freeze and then remelted, bubbles would reappear.

The concentration range covered had an upper limit dictated by the difficulty of preparing a bubble-free solution; the lower limit was established by the fact that the rotational motion became so rapid that the depolarized Rayleigh component was extremely broad, creating signal-to-noise problems. The temperature range was restricted at the high end (60°C) by the loss of water and at the low end by the fact that the rotational motion became so slow that broadening could not be measured.

Overlap of depolarized components from adjacent orders can cause significant uncertainty in placing the baseline which can in turn lead to errors in the half-width measurements. Overlap becomes more serious as the free spectral range is decreased (24). A free spectral range was employed such that the observed half-width was approximately 0.1-0.2 of a free spectral range - a procedure similar to that of Phillies and Kivelson (25). As a result, little error is expected from the procedure of taking the zero as the minimum of the observed intensity curve, which occurred at a point midway between adjacent depolarized Rayleight components. The instrumental line shape was determined by recording a polarized spectrum of light scattered elastically by an aqueous polystyrene sphere suspension contained in a cell identical to the sample cell. This spectrum was immediately recorded before and after that of the sample in order to assess any effect of equipment instability. Since the whole sequence

was completed within 13 to 15 minutes, drift and deterioration of finesse did not prove to be a problem. The spectra were always recorded at high sweep rates with a very good Houston 2000 recorder so that linewidths could be reliably amplified for ease of measurement. The depolarized linewidth was often several times greater than the instrumental linewidth.

A number of spectra were analyzed with a Hewlett Packard (HP) 9835A Desktop computer. This necessitated first digitizing the instrumental and depolarized spectra from the analog recordings with a HP 9874A digitizer or a HP 9872A Digital Plotter if equal frequency intervals between points were required. In the course of this digitization the spectra were visually smoothed.

The shear viscosities which were not available in the literature were determined by a calibrated Cannon-Ubbelohde viscometer.

III. RESULTS AND DISCUSSION

A typical depolarized spectrum together with the corresponding polarized spectrum and zero level are shown in Figure 1. As was mentioned earlier, the Rayleigh wings appear as a flat background, consisting of overlapping adjacent spectral orders within the free spectral range employed. No substructure (i.e., no doublet) was observed in the central component, indicating that scattering from the overdamped shear mode which couples to orientational fluc-tuations is either not occurring or not making a measurable contribution.

In Figure 2, one of the depolarized components taken from Figure 1 has been fit, using a nonlinear regression program, to a single Lorentzian plus a baseline. The sum of the squares of the residuals for the fit is 0.0095.

We would expect the NO_3^- ion, which has D_{3h} symmetry and which is an oblate ellipsoid, to give rise to a depolarized spectrum consisting of two

Lorentzians (26). The moment of inertia about the C_3 axis is 1.19 x 10^{-38} g cm^2 while the two equal moments of inertia about the axes which lie in the plane of the atoms and which are perpendicular to the C_3 axis are one half this value. The fact that the depolarized spectrum can be fit to a single Lorentzian implies that rotation about these latter two axes gives rise to the depolarized spectrum. Rotation about the C_3 axis does not affect the depolarized Rayleigh linewidth, since the polarizability of the NO_3^- ion is isotropic about this axis.

In Figure 3 the instrumental profile has also been fitted to a single Lorentzian. The sum of the squares of the residuals in this case is 0.048. Others have been able to fit their instrumental profile to a single Lorentzian function (27). This instrumental response function is a convolution of the laser profile and the interferometer profile, and, as shown by Leidecker and LaMacchia (28), it is in general best approximated by a Voigt function, which is characterized by a Lorentzian and a Gaussian part. In several studies a ratio of the Lorentzian fraction to the Gaussian fraction of about 0.5 has been reported (28, 29). The Gaussian contribution can result in the instrumental profile having wings slightly more compressed than that of a pure Lorentzian. Any misalignment of the interferometer and/or the pinhole preceding the photomultiplier will distort the instrumental profile so that it can no longer be approximated by a Voigt function. This instrumental profile is folded with the actual distribution of the scattered light to produce the experimentally measured spectrum.

In view of the finding that the depolarized and instrumental profiles were closely described by Lorentzian functions, a good approximation to the depolarized Rayleigh semi-halfwidth with instrumental broadening removed, Γ,

was obtained by subtracting the instrumental semi-halfwidth from the recorded depolarized Rayleigh semi-halfwidth. A further refinement to the value of Γ was made to account for the departure of the instrumental function from pure Lorentzian character due to the reasons cited above. This was accomplished by making use of the procedure (as well as a BASIC version of the exact program) described by Pine (30). This procedure entails convoluting generalized Lorentzian functions with the digitized instrumental profile until a match is obtained between the semi-halfwidth of the convoluted spectrum and that of the recorded spectrum. The computer generated values were an average of 6% greater than the Lorentzian semi-halfwidths obtained by straightforward subtraction. Pine (30) found a 10% difference, but he was dealing with Brillouin components of the polarized spectrum where component overlap results in a greater background subtraction error than encountered here with the depolarized spectrum. Since the spectra reported on here were obtained in the form of analog recordings and not all were suitable for computer analysis, the 6% correction factor was applied uniformly.

Considering the many possible sources of error in determining Γ, which include spectral noise, interferometer instability, errors in placing the baseline, errors in the above outlined deconvolution procedure, temperature and free spectral range uncertainties, as well as possible contributions from stray light and leakage of the polarized spectrum, an overall error in Γ is difficult to estimate. A conservative estimate would place this error somewhere between $\pm$ 5% and $\pm$ 10%.

Using these values of Γ, corrected for instrumental broadening, the rotational relaxation time, τ, was computed from the formula

$$\tau = \frac{1}{2\pi\Gamma}$$

(6)

8

The values of τ, along with the required values of the shear viscosity η_s, appear in Tables 1 and 2.

In Figure 4, Arrhenius plots for the $Ca(NO_3)_2$ solutions and $Zn(NO_3)_2 \cdot 5$ H_2O solution are depicted. The data for all the solutions except the $Ca(NO_3)_2 \cdot 3.91$ H_2O could be least squares fitted to straight lines. The parameters for these lines are given in Table 3. Also given in Table 3 is the apparent activation energy E_a for rotation which appears in the equation

$$\tau = \tau_o \exp (E_a/RT) \tag{7}$$

where τ_o is a constant, R is the gas constant, and T is the absolute temperature.

The activation energy for nitrate rotation, as can be seen, is very similar for $Ca(NO_3)_2 \cdot 4.0$ H_2O and $Zn(NO_3)_2 \cdot 5.0$ H_2O. However, the activation energies for the $Ca(NO_3)_2$ solutions show a fairly significant change in going from 5 H_2O to 4 H_2O. This could be due to a structural change. One possibility is the rearrangement of the coordination sphere of the cation; for example, the transition from one nitrate to two nitrates. On the basis of vibrational spectroscopic data, it has been inferred that contact ion pairs between Zn^{+2} and NO_3^- are formed when the water-to-salt ratio, X, drops below 6 (31). Using the same ν_4 (E') band splitting criterion, Ca^{+2} forms inner-sphere complexes with NO_3^- when $X \le 6$ (32).

The range of temperature as well as viscosity covered by the measurements for $Ca(NO_3)_2 \cdot 3.9$ H_2O is greater than for any of the other liquids studied, consequently the non-linear behavior in Figure 4 is not at all surprising. In fact, this same non-linear behavior would be expected for the other solutions as well if the temperature range were extended. Our measurements for $Ca(NO_3)_2 \cdot 3.91$ H_2O have entered the upper end of the

supercooled region. Since the three parameter Vogel-Tamman-Fulcher equation has been used extensively in fitting the transport properties of various hydrate melts (33), it was selected for fitting the $Ca(NO_3)_2 \cdot 3.91 \, H_2O$ data. In terms of τ, this equation can be expressed as

$$\tau = AT^{\frac{1}{2}} \exp \left(\frac{B}{T-T_o}\right) \tag{8}$$

where A, B, and T_o are parameters. The parameter T_o has been given physical significance by the free volume theory of Cohen and Turnbull whereby T_o is the "ideal" glass transition temperature at which the free volume of the liquid disappears and liquid transport becomes impossible (34). In the alternate theory of Adams and Gibbs (35) T_o is the temperature at which the configurational entropy of the supercooled liquid becomes zero.

The experimental values of τ were non-linear least squares fitted to the logarithmic form of the preceding equation, namely

$$\log \tau = \frac{1}{2.303} \left(\frac{B}{T-T_o}\right) - \frac{1}{2} \log T + C \tag{9}$$

where $C = \log A$. The fitted values are $B = 438.59°K$, $C = -22.14$, and $T_o = 203.75°K$. A plot of $\log \tau + \frac{1}{2} \log T$ is shown in Figure 5. The expected straight linge shows the goodness of the fit. This value of T_o is quite reasonable, considering that Moynihan (36) has determined a value of 205°K for $Ca(NO_3)_2 \cdot 4 \, H_2O$ from shear viscosity data. Angell and Moynihan, however, have pointed out that in order to obtain precise values of T_o and B, the transport data must extend over several orders of magnitude (33).

Angell and Moynihan also have reported that the composition studies of $Ca(NO_3)_2 \cdot X \, H_2O$ (X = 4 to 7) yield results consistent with the B for equivalent conductance of 590°K and the B for shear viscosity of 690°K (33).

10

In the case of $Ca(NO_3)_2 \cdot 4 H_2O$ the mean activation energy for shear viscosity η_s, evaluated over the range of 25° - 70°C, is approximately 10.6 Kcal/mole (37). Clearly, the barriers to migration and viscous flow in these liquids are greater than for rotational motion of the NO_3^- ion. In the Raman spectroscopic study of the rotation motion of the NO_3^- ion in monovalent nitrate melts by Ponyatenko and Radchenko (38), the energy of activation was also found to be less than that for visous flow. This was interpreted to mean that the rotational motion of a NO_3^- ion in nitrate melts can be represented in the form of rotational oscillations relative to an equilibrium position, accompanied by occasional turns with a change in orientation. An extensive analysis of the activation energies of translation determined from NMR measurements, E_{trans}, with those of rotational E_{rot}, and viscous flow, E_{η_s}/T, of organic liquids (39) indicated that $E_{trans} = E_{\eta_s}/T > E_{rot}$, revealing that the viscosity of a liquid depends to a larger extent on the frequency of the translational, rather than orientational, jumps of molecules.

As has already been mentioned, the actual relationship between the rotational reorientation time τ and the shear viscosity is of special interest. In this regard two different types of plots have been made. First in Figures 6 and 7, τ is plotted versus η_s for $Ca(NO_3)_2 \cdot X H_2O$ at 40°C and $Zn(NO_3)_2 \cdot X H_2O$ at 50°C, respectively. In both cases the rotational reorientation time τ varied due to a variation in water concentration; that is, the solute - solvent ratio with the nitrate ion being considered the solute were varied. The values of η_s for Figure 5 were taken from the data by Bak (40). Notice in Table 1 that the three experimental values of η_s for $Ca(NO_3)_2 \cdot 4 H_2O$ which were determined by different investigators do not agree. The values of η_s for the $Zn(NO_3)_2$ solutions which were used in Figure 6 were determined in

11

this study. Both of these plots have been fitted to straight lines with non-zero intercepts. The equations for these straight lines are given in Table 3.

In the second type of plot, which is shown in Figure 7, τ is plotted as a function of η_s/T for $Ca(NO_3)_2 \cdot 4 H_2O$. Again a linear dependence is found. In this case, however, the composition, i.e. X, is fixed and the variation of τ and η_s with temperature is considered. It should be noted that the shear viscosity values employed in Figure 7 are those of Moynihan (36). The parameters obtained by linear regression analysis appear in Table 3.

Comparisons between the experimental slopes C_{exp} of Figures 5 and 6 and the slopes calculated using stick and slip boundary conditions are given in Table 4. Also given in Table 4 is a comparison between the experimental C' obtained from Figure 7 and the values calculated again using stick and slip boundary conditions. It is apparent from equations 1, 2 and 4 that

$$C_{stick} = \frac{V}{kT} \left(\frac{f}{f_o}\right) \tag{10}$$

Values of $V = 25 \overset{\circ}{A}^3$ and $(a/b) = 0.48$ were employed in these calculations. These values were based on the disk-like model of the nitrate ion proposed by Janz and James (41,42). From the a/b ratio and the paper by Edwards (13), it follows that $f/f_o = 1.04$.

C_{slip} can be calculated using the equation

$$C_{slip} = \frac{\lambda V}{8\rho_x \rho_y kT} \tag{11}$$

while $C'_{slip} = C_{slip}T \tag{12}$

where λ is a slip friction coefficient and ρ_x and ρ_y are ellipsoid axial ratios which are defined as the ratio of the given axis to the longest axis. Again using the dimensions specified by Janz and James (41,42), $\rho_x = 0.48$ and $\rho_y = 1$. Using either reference 19 or 20, a friction coefficient of $\lambda = 1.28$ is obtained.

An alternate way is to use available tabulated values of C_{slip}/C_{stick} 19).

For an oblate ellipsoid of axial ratio 0.48, one obtaines $C_{slip}/C_{stick} =$ 0.29. Using the values of C_{stick} or C'_{stick}, it is an easy matter to compute C_{slip} or C'_{slip}.

Table 4 reveals that stick boundary conditions result in a value of C or C' which is too high. This prediction of too much friction has been the general finding for stick boundary conditons. The slip boundary conditions, however, underestimate C or C', and consequently the friction coefficient as well. The ratios between the C_{exp} and C_{stick} and C_{slip} for $Ca(NO_3)_2 \cdot$ X H_2O and $Zn(NO_3)_2 \cdot$ X H_2O are very similar; even this difference could be attributed to experimental error and uncertainties in the values of η_s. The stick boundary conditions appear to be more applicable in these two cases. However, the slip boundary conditions yield a value far closer to C_{exp} for the $Ca(NO_3)_2 \cdot$ 4 H_2O experiment in which the temperature was varied.

An explanation for these conflicting findings is not completely apparent. In the first type of experiment in which X was varied at constant temperature, the pair correlations are expected to vary considerably more than in the constant temperature experiment for $Ca(NO_3)_2 \cdot$ 4 H_2O. Perhaps stick boundary conditions are able to account for these changes in pair correlations more effectively than slip boundary conditions, while slip boundary conditions are more applicable for constant composition in which the temperature is varied and in which pair correlations play less of a role. In any event, it can be concluded that the NO_3^- rotation is under viscous control and the experimental values of C or C' lie between the values predicted by the stick and slip boundary conditions.

13

Moynihan and Angell (43) have interpreted their results on the chrono-potentiometric diffusion coefficients of Ag+, Tl+, and Cd+2 ions in molten $Ca(NO_3)_2 \cdot 4 H_2O$ in terms of the Stokes-Einstein equation. It was found that for a given value of η_s there exist a correlation betweem the diffusion coefficient and ionic radius. At a given temperature the agreement between the observed and calculated diffusion coefficients for Ag+, Tl+, and $Cd(H_2O)_4^{+2}$ were fairly good. Unfortunately, the quality of this comparison is questionable in view of the criticism by Lovering (44), who contends that Moynihan and Angell did not collect their data under strict diffusion control.

It is also interesting to note that the value of the free rotator correlation time for the NO_3^- ion, calculated using equation (5), is 2.5×10^{-13} sec. This value is considerably shorter than the intercept values which were found in this study. (Refer to Table 3).

A comparison between the values of τ for $Ca(NO_3)_2 \cdot 5.0 H_2O$ and $Zn(NO_3)_2 \cdot 5.0 H_2O$ at 50°C reveals that rotational motion is 1.6 times slower in $Ca(NO_3)_2$ than the corresponding $Zn(NO_3)_2$ solution, even though the value of E_a is 5.6 Kcal/mole for the $Ca(NO_3)_2$ solution and 8.3 Kcal/mole for the $Zn(NO_3)_2$ solution. This can be explained on the basis of the higher viscosity for the $Ca(NO_3)_2$ solution and remembering that nitrate rotation is under viscous control. The higher viscosity of the $Ca(NO_3)_2$ solution can in turn be accounted for by the more ionic nature of the $Ca^{+2} - NO_3^-$ bonds.

In our analysis we have neglected the effects of orientational pair correlations. We have assumed that the broadening of the depolarized Rayleigh component was entirely attributable to single anion reorientation; i.e., we have employed the single-particle Brownian rotational diffusion picture. Rayleigh scattering is a coherent process so the depolarized spectrum contains information about correlated molecular reorientation. One method of gaining additional insight into the pair interactions is to compare the results of

14

Raman and depolarized Rayleigh scattering. Raman scattering is an inco-
herent process, and the width of the Raman band is determined only by
vibrational and reorientational relaxations of single molecules (45). An
alternate approach is to compare the NMR reorientational correlation time
(which is also a single molecule relaxation time) with the results of
depolarized light scattering (46). Such experiments are now in progress.

IV. ACKNOWLEDGEMENTS
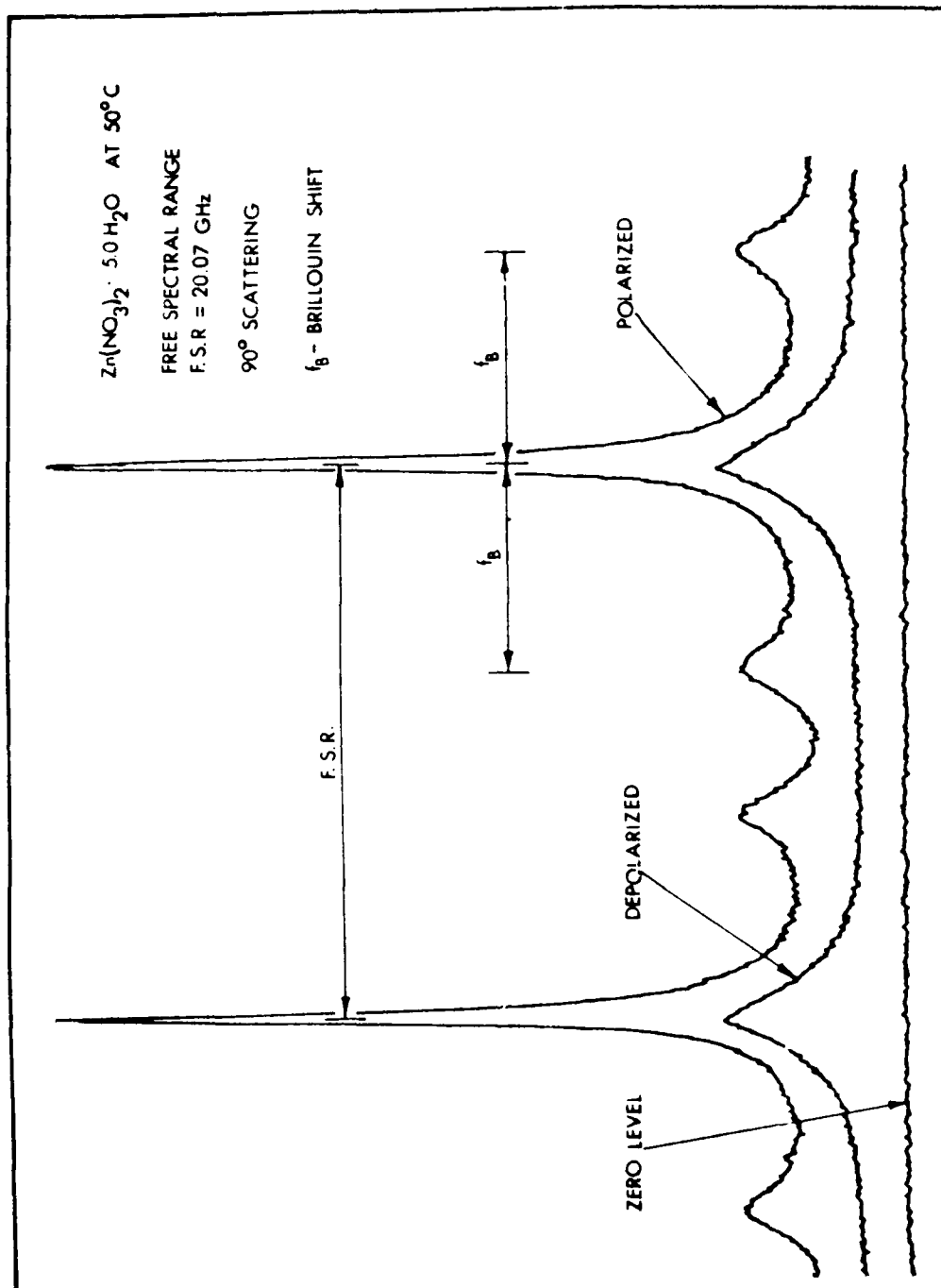
Fig. 1 Superimposed polarized and depolarized spectra for $Zn(NO_3)_2$ $\cdot$ 5.0 H_2O along with zero level.

Text within the figure:

$Zn(NO_3)_2 \cdot 5.0\,H_2O$ AT 50°C

FREE SPECTRAL RANGE
F.S.R = 20.07 GHz

90° SCATTERING

f_B – BRILLOUIN SHIFT

POLARIZED

DEPOLARIZED

ZERO LEVEL

F.S.R.

f_B

f_B
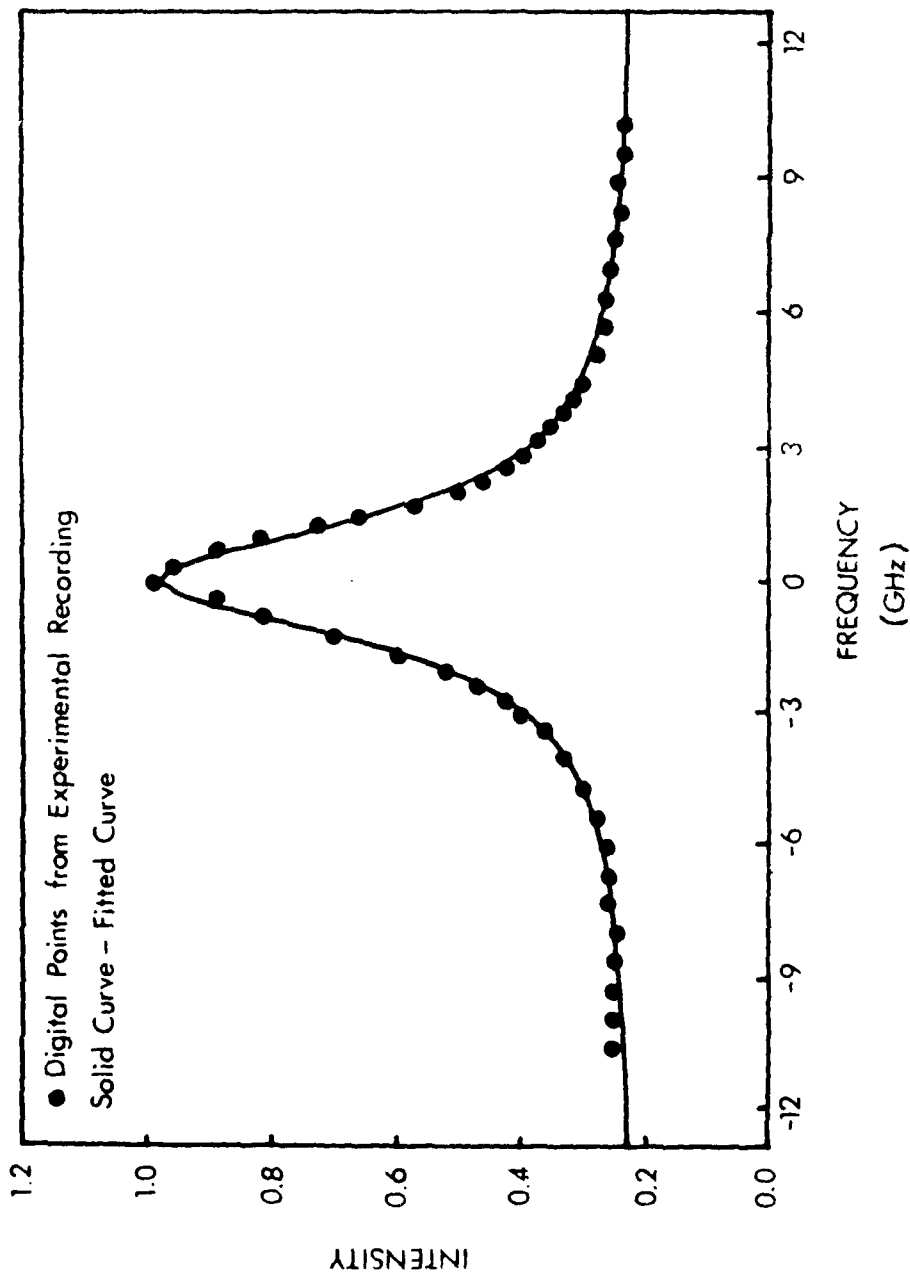
Fig. 2 Fit of calculated and digitized depolarized spectra. The points are digitized data taken from the analog spectrum in Figure 1. The solid line is the calculated fit to one Lorentzian plus a baseline.
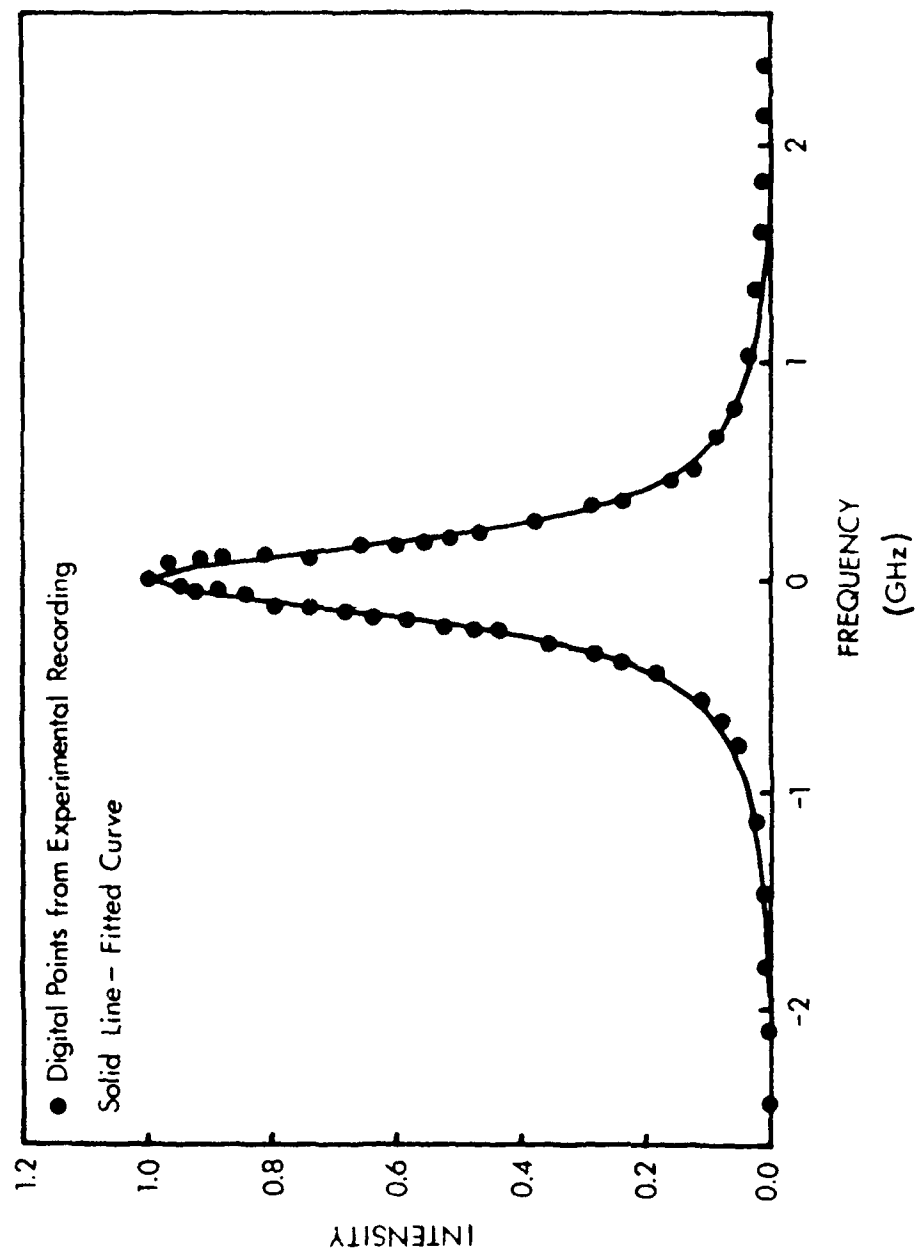
Fig. 3 Fit of calculated and digitized instrumental spectra. The instrumental profile is that for the spectra in Figure 1. The solid line is a calculated fit to one Lorentzian.
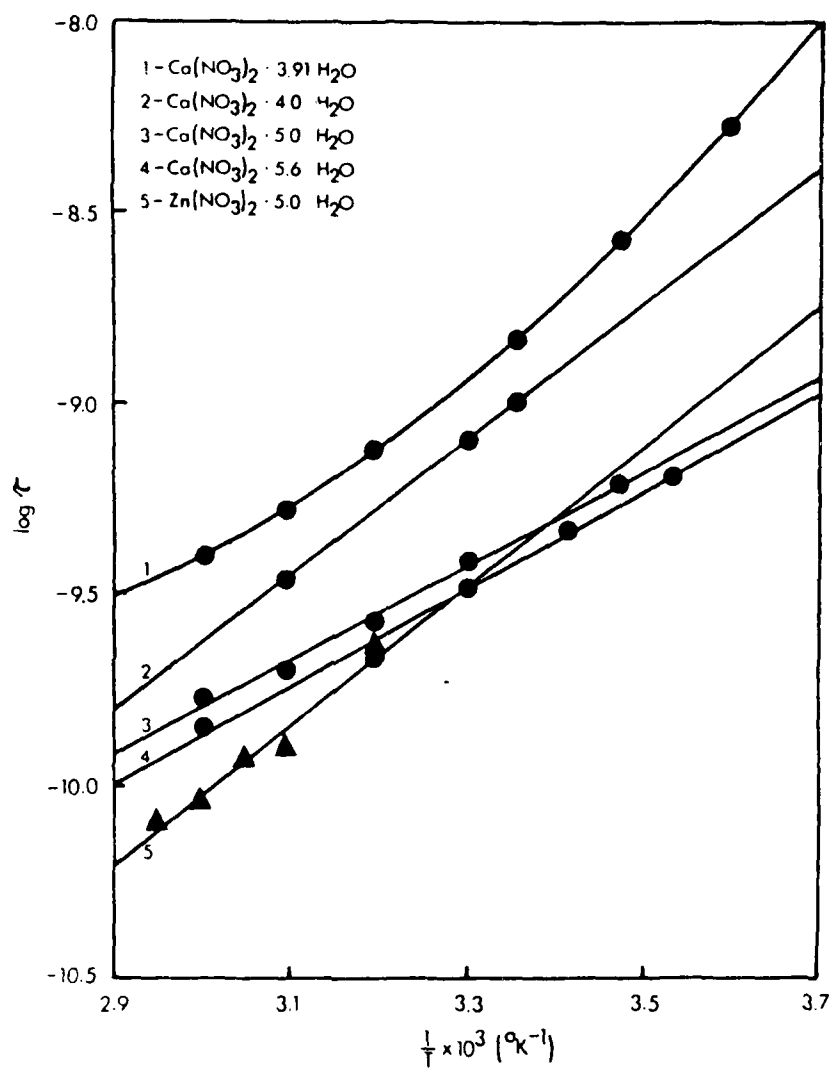
Fig. 4 Arrhenius plots for $Ca(NO_3)_2 \cdot X\ H_2O$ and
$Zn(NO_3)_2 \cdot 5.0\ H_2O$

- 20 -
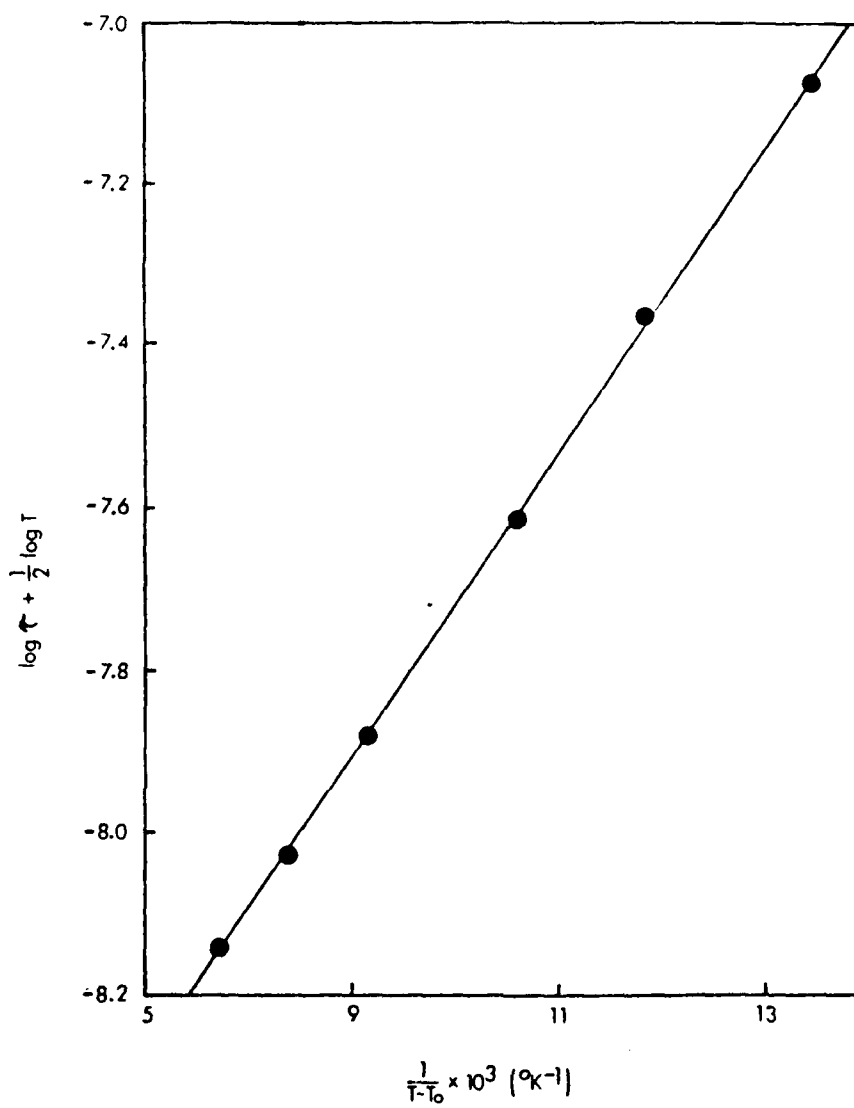
Fig. 5. Vogel-Tammann-Fulcher plot for $Ca(NO_3)_2 \cdot 3.91\,H_2O$.
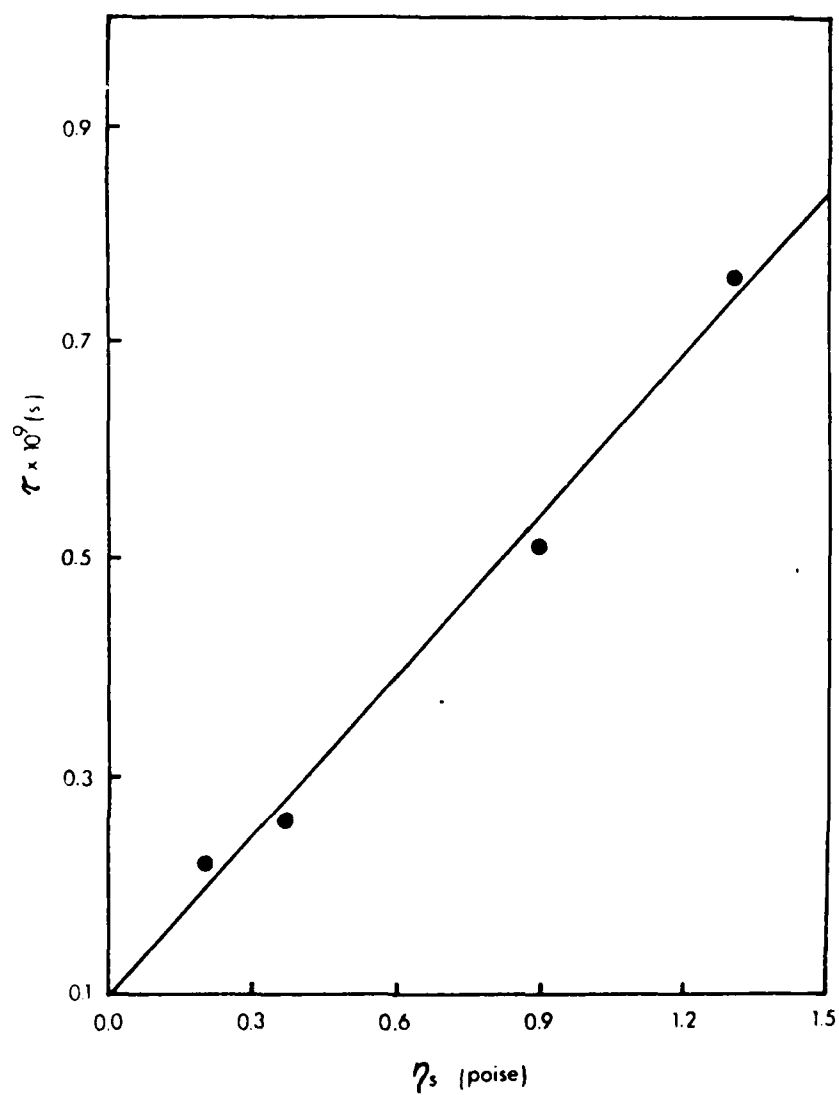
Fig. 6. Rotational relaxation time versus shear viscosity for $Zn(NO_3)_2 \cdot X H_2O$ at 40°C.
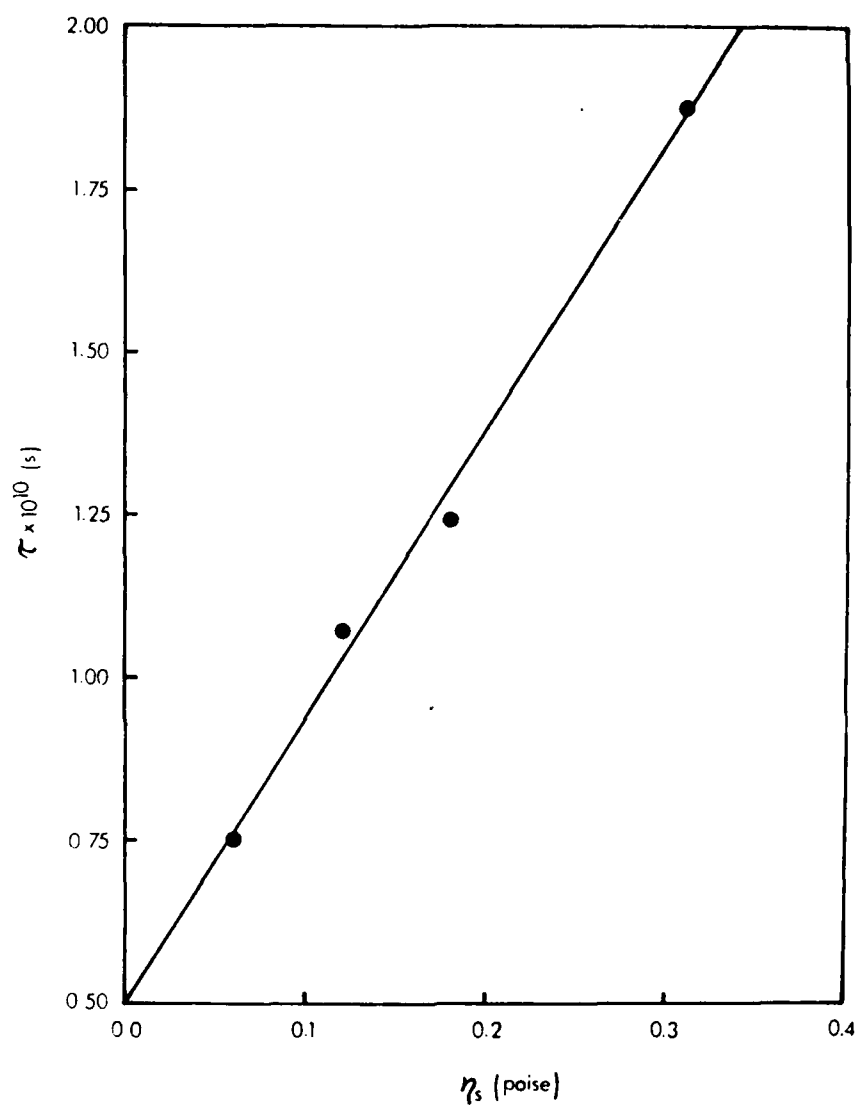
Fig. 7. Rotational relaxation time versus shear viscosity for $Zn(NO_3)_2 \cdot X\ H_2O$ at 50°C.
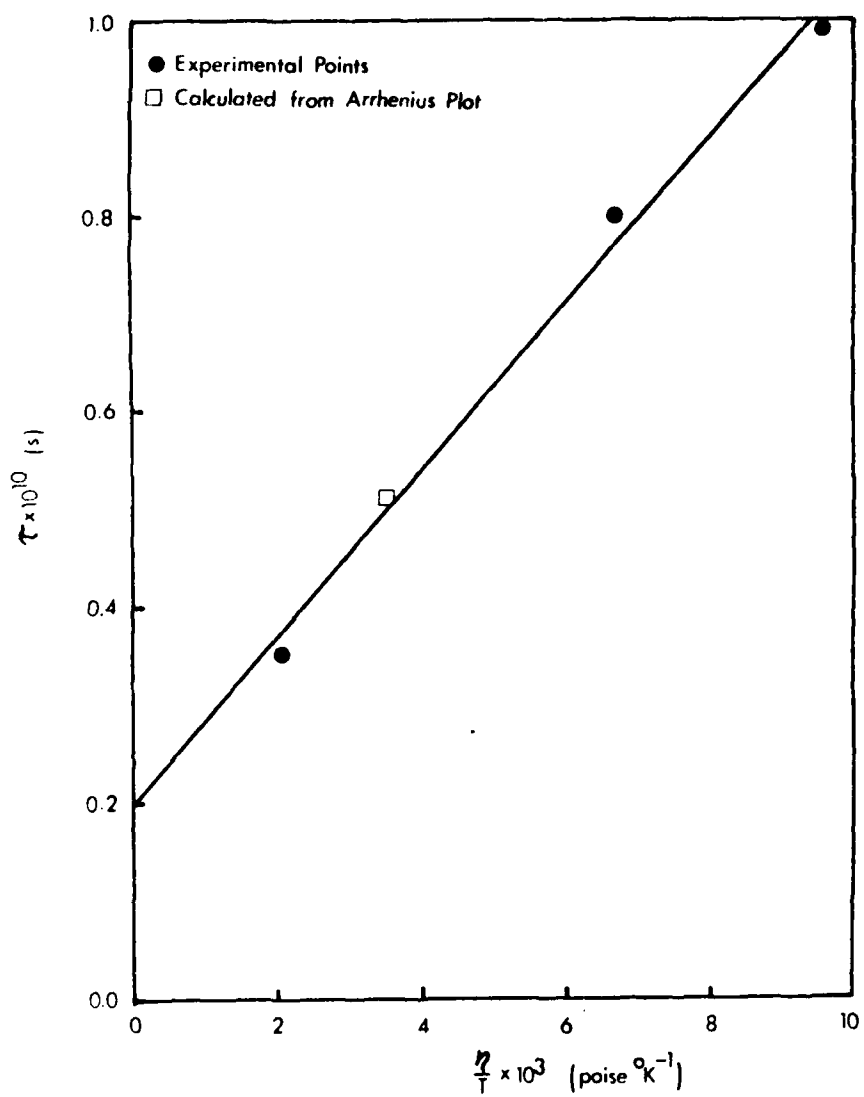
Fig. 8. Rotational relaxation time versus η_s/T for $Ca(NO_3)_2 \cdot 4 H_2O$.

TABLE 1. Experimental Data for $Ca(NO_3)_2 \cdot X\ H_2O$

X	t(°C)	$\tau \times 10^9$ (s)	η_s (poise)	
3.91	5	5.3		
	15	2.65		
	25	1.45		
	40	0.76	1.30	(40)
	50	0.53		
	60	0.40		
4.0	25	0.99	2.85	(36)
	30	0.80	2.03	(36)
	40	0.51*	1.101	(36)
			1.062	(47)
			0.819	(40)
	50	0.35	0.669	(36)
5.0	15	0.62		
	30	0.38		
	40	0.26	0.365	(40)
	50	0.20		
	60	0.17		
5.6	10	0.64		
	20	0.47		
	30	0.32		
	40	0.22	0.198	(40)
	60	0.14		

*Determined from log τ vs. 1/T plot

TABLE 2. Experimental Data for $Zn(NO_3)_2 \cdot X\ H_2O$

X	t(°C)	$\tau \times 10^{10}$ (s)	η_s (poise)
3.8	50	1.87	0.31
5.0	40	2.27	0.18
	50	1.24	
	55	1.17	
	60.5	0.91	
	66	0.80	
6.0	50	1.07	0.12
8.0	50	0.75	0.06

TABLE 3

Solution	Least Squares Line	*Standard Error of Estimate	Ea(Kcal/mole)
Figure 4			
$Ca(NO_3)_2 \cdot 4\ 0\ H_2O$	$\log \tau = 1770(1/T)-14.94$	0.15	8.1
$Ca(NO_3)_2 \cdot 5\ 0\ H_2O$	$\log \tau = 1233(1/T)-13.50$	2.30	5.6
$Ca(NO_3)_2 \cdot 5\ 6\ H_2O$	$\log \tau = 1280(1/T)-13.71$	2.52	5.8
$Zn(NO_3)_2 \cdot 5\ 0\ H_2O$	$\log \tau = 1825(1/T)-15.50$	3.82	8.3
Figure 6			
$Ca(NO_3)_2 \cdot X\ H_2O$	$\tau = (4.95 \times 10^{-10})\ \eta_s + 9.70 \times 10^{-11}$	3.24	
Figure 7			
$Zn(NO_3)_2 \cdot X\ H_2O$	$\tau = (4.39 \times 10^{-10})\ \eta_s + 4.97 \times 10^{-11}$	4.80	
Figure 8			
$Ca(NO_3)_2 \cdot 4 \cdot 0\ H_2O$	$\tau = (8.54 \times 10^{-8})\ \eta_s/T + 1.96 \times 10^{-10}$	3.35	

* If x_I, y_i are the values of the independent and dependent variables, respectively, measured in the course of the experiment and $y_i = b_o + b_i x_i$ is the fitted equation where b_o and b_1 are parameters, then the standard error of the estimate is equal to the expression

$$\sqrt{\frac{[\Sigma yi - (b_o + b_1 yi)]^2}{n-2}}$$

n = number of experimental points.

TABLE 4

Solution	C_{exp} $\times 10^{10}$ s/poise	C_{stick} $\times 10^{10}$ s/poise	C_{slip} $\times 10^{10}$ s/poise
$Ca(NO_3)_2 \cdot X\ H_2O$ $T = 40°C$	4.95	6.01	1.50
$Zn(NO_3)_2 \cdot X\ H_2O$ $T = 50°C$	4.39	5.83	1.46

	C'_{exp} $\times 10^8\ \dfrac{s\ °K}{poise}$	C'_{stick} $\times 10^8\ \dfrac{s\ °K}{poise}$	C'_{slip} $\times 10^8\ \dfrac{s\ °K}{poise}$
$Ca(NO_3)_2 \cdot 4\ H_2O$	8.54	18.8	5.45

REFERENCES

1. R. A. Carpio, F. Borsay, C. Petrovic, and E. Yeager, J. Chem. Phys. $\underline{65}$, 29 (1976).

2. C. A. Angell, J. Electrochem. Soc. $\underline{112}$, 1224 (1965).

3. J. Braunstein, Inorg. Chim. Acta Reviews $\underline{2}$, 19 (1968).

4. C. A. Angell, Ann. Rev. Phys. Chem. $\underline{22}$, 429 (1971).

5. N. P. Bansal and J. A. Plambeck, Electrochim. Acta $\underline{23}$, 1053 (1978).

6. N. P. Bansal and J. A. Plambeck, Electrochim. Acta $\underline{23}$, 679 (1978).

7. B. D. Kurnikov and T. Hurlen, J. Electroanal. Chem. $\underline{91}$, 367 (1978).

8. D. R. Bauer, J. I. Brauman, and R. Pecora, Ann. Rev. Phys. Chem. $\underline{27}$, 443 (1976).

9. A. I. Prorvin, Optics and Spectroscopy $\underline{28}$, 140 (1969).

10. W. A. Steele, Adv. in Chem. Phys. $\underline{34}$, 1 (1976).

11. A. Einstein, Investigations on the Theory of the Brownian Movement, Dover, New York, NY, 1956.

12. F. Perrin, J. Phys. Radium $\underline{7}$, 1 (1936).

13. J. T. Edward, J. Chem. Ed. $\underline{47}$, 261 (1970).

14. D. R. Jones and C. H. Wang, J. Chem. Phys. $\underline{66}$, 1659 (1977).

15. C. H. Wang, D. R. Jones, and D. H. Christenson, J. Chem. Phys. $\underline{64}$, 2820 (1976).

16. C. K. Cheung, D. R. Jones, and C. H. Wang, J. Chem. Phys. $\underline{64}$, 3567 (1976).

17. G. R. Alms, D. R. Bauer, J. I. Brauman, and R. Pecora, J. Chem. Phys. $\underline{58}$, 5570 (1973).

18. F. J. Bartoli and T. A. Litovitz, J. Chem. Phys. $\underline{56}$, 413 (1972).

19. C. Hu and R. Zwanzig, J. Chem. Phys. $\underline{60}$, 4353 (1974).

20. G. K. Youngren and A. Acrivos, J. Chem. Phys. $\underline{63}$, 3846 (1975).

21. D. R. Bauer, J. I. Brauman, and R. Pecora, J. Amer. Chem. Soc. $\underline{96}$, 6840 (1974).

22. D. H. Rank, A. Hollinger, and D. P. Eastman, J. Opt. Soc. Am. $\underline{56}$, 1057 (1966).

23. S. I. Smedley, C. Hall, and E. Yeager, J. Phys. Chem. 76, 1506 (1972).

24. H. C. Craddock, D. A. Jackson, and J. G. Powles, Mol. Phys. 14, 373 (1968).

25. G. D. J. Phillies and D. Kivelson, J. Chem. Phys. 71, 2575 (1979).

26. R. Pecora, J. Chem. Phys. 49, 1036 (1968).

27. L. Boyer, R. Vacher, L. Cecchi, M. Adam and P. Berge, Phys. Rev. Letters 26, 1435, (1971).

28. H. W. Leidecker and J. LaMacchia, J. Acoust. Soc. Amer. 43, 143 (1968).

29. G. R. Alms, D. R. Bauer, J. I. Brauman, and R. Pecora, J. Chem. Phys. 59, 5321 (1973).

30. A. S. Pine, Phys. Rev. 185, 1187 (1969).

31. D. E. Irish, A. R. Davis, and R. A. Plane, J. Chem. Phys. 50, 2262 (1969).

32. R. E. Hester and R. A. Plane, J. Chem. Phys. 40, 411 (1964).

33. C. A. Angell and C. T. Moynihan, in Molten Salts, Characterization and Analysis, G. Mamantov, Editor, Marcel Dekker, New York (1969).

34. M. H. Cohen and D. Turnbull, J. Chem. Phys. 31, 1164 (1959); ibid, 34, 120 (1961).

35. G. Adams and J. H. Gibbs, J. Chem. Phys. 43, 139 (1965).

36. C. T. Moynihan, J. Phys. Chem. 70, 3399 (1966).

37. C. T. Moynihan, J. Chem. Ed. 44, 531 (1967).

38. N. A. Ponyatenko and I. V. Radchenko, Opt. Spectroscopy 26, 353 (1969).

39. F. M. Samigullin, Zhurnal Strukturnoi Khimii 14, 611 (1973).

40. B. V. Bak, Zh. Fiz. Khim. 13, 534 (1939).

41. G. J. Janz and D. W. James, J. Chem. Phys. 35, 739 (1961).

42. G. J. Janz and D. W. James, Electrochim. Acta 7, 427 (1962).

43. C. T. Moynihan and C. A. Angell, J. Phys. Chem. 74, 736 (1970).

44. D. G. Lovering, Collect. Czech. Chem. Commun. 37, 3697 (1972).

45. C. K. Cheung, D. R. Jones, and C. H. Wang, J. Chem. Phys. 64, 3567 (1976).

46. G. R. Alms, D. R. Bauer, J. I. Brauman, and R. Pecora, J. Chem. Phys. 59, 5310 (1973).

47. G. S. Darbari and S. Petrucci, J. Phys. Chem. 73, 921 (1969).

TECHNICAL REPORT DISTRIBUTION LIST

CASE WESTERN RESERVE UNIVERSITY

Contract N00014-75-C-0557   Project NR 384-305

Director   3 copies
Defense Advanced Research Projects Agency
Attn: Technical Library
1400 Wilson Blvd.
Arlington, Virginia 22209

Office of Naval Research   3 copies
Physics Program Office (Code 421)
800 North Quincy Street
Arlington, Virginia 22217

Office of Naval Research   1 copy
Assistant Chief for Technology (Code 200)
800 North Quincy Street
Arlington, Virginia 22217

Naval Research Laboratory   3 copies
Depdrtment of the Navy
Attn: Technical Library
Washington, D.C. 20375

Office of the Director of Defense   3 copies
    Research and Engineering
Information Office Library Branch
The Pentagon
Washington, D.C. 20301

U.S. Army Research Office   2 copies
Box 12211
Research Triangle Park
North Carolina 27709

Defense Documentation Center   12 copies
Cameron Station (TC)
Alexandria, Virginia 22314

Director, National Bureau of Standards   1 copy
Attn: Technical Library
Washington, D.C. 20234

Commanding Officer   3 copies
Office of Naval Research Branch Office
536 South Clark Street
Chicago, Illinois 60605

Commanding Officer   3 copies
Office of Naval Research Branch Office
1030 East Green Street
Padadena, Cdlifornia 91101

-31-

San Francisco Area Office   3 copies
Office of Naval Research
One Hallidie Plaza
Suite 601
San Francisco, California 94102

Commanding Officer   3 copies
Office of Naval Research Branch Office
666 Summer Street
Boston, Massachusetts 02210

New York Area Office   1 copy
Office of Naval Research
715 Broadway, 5th Floor
New York, New York 10003

Director   1 copy
U. S. Army Engineering Research
    and Development Laboratories
Attn: Technical Documents Center
Fort Belvoir, Virginia 22060

ODDR&E Advisory Group on Electron Devices   3 copies
201 Varick Street
New York, New York 10014

Air Force Office of Scientific Research   1 copy
Department of the Air Force
Bolling AFB, D.C. 22209

Air Force Weapons Laboratory   1 copy
Technical Library
Kirtland Air Force Base
Albuquerque, New Mexico 87117

Air Force Avionics Laboratory   1 copy
Air Force Systems Command
Technical Library
Wright-Patterson Air Force Base
Dayton, Ohio 45433

Lawrence Livermore Laboratory   1 copy
Attn: Dr. W. F. Krupke
University of California
P.O. Box 808
Livermore, California 94550

Harry Diamond Laboratories   1 copy
Technical Library
2800 Powder Mill Road
Adelphia, Maryland 20783

Naval Air Development Center   1 copy
Attn: Technical Library
Johnsville
Warmister, Pennsylvania 18974

Naval Weapons Center   1 copy
Technical Library (Code 753)
China Lake, California 93555

Naval Training Equipment Center   1 copy
Technical Library
Orlando, Florida 32813

Naval Underwater Systems Center   1 copy
Technical Library
New London, Connectivut 06320

Commandant of the Marine Corps   1 copy
Scientific Advisor (Code RD-1)
Washington, D.C. 20380

Naval Ordnance Station   1 copy
Technical Library
Indian Head, Maryland 20640

Naval Postgraduate School   1 copy
Technical Library (Code 0212)
Monterey, California 93940

Naval Missile Center   1 copy
Technical Liorary (Code 5632.2)
Point Mugu, California 93010

Naval Ordnance Station   1 copy
Technical Library
Louisville, Kentucky 40214   1 copy

Commanding Officer   1 copy
Naval Ocean Research & Development Activity
Technical Library
NSTL Station, Mississippi   39529

Naval Explosive Ordnance Disposal Facility   1 copy
Technical Library
Indian Head, Maryland 20640

Naval Ocedn Systems Center   1 copy
Technical Library
San Diego, California   92152

Naval Surface Weapons Center
Technical Library
Dahlgren, Virginia 22448   1 copy

Naval Surface Weapons Center (White Oak)   1 copy
Technical Library
Silver Spring, Maryland 20910

Naval Ship Research and Development Center   1 copy
Central Library (Code L42 and L43)
Bethesda, Maryland 20084

Naval Avionics Facility   1 copy
Technical Library
Indianapolis, Indiana 46218

END

DATE
FILMED

3-81

DTIC